Hindawi
Journal of Electrical and Computer Engineering
Volume 2024, Article ID 7070078, 12 pages
https://doi.org/10.1155/2024/7070078

Research Article

Suppression Method for Smeared Spectrum Jamming Based on Lv's Distribution Combined with Biorthogonal Fourier Transform

Zhenming Wen, Guohong Wang, and Hongbo Yu

Institute of Information Fusion, Naval Aviation University, Yantai 264001, China

Correspondence should be addressed to Zhenming Wen; 935838465@qq.com

Received 20 November 2023; Revised 23 December 2023; Accepted 9 January 2024; Published 22 January 2024

Academic Editor: Andrea Tani

Smeared spectrum (SMSP) jamming is a deceptive jamming technique commonly used against linear frequency modulation (LFM) radar. This technique produces high-density false targets that resemble a comb shape after pulse compression processing, resulting in both deceiving and suppressing effects. In order to suppress jamming effectively, a new antijamming technique has been proposed that combines Lv's distribution (LVD) with biorthogonal Fourier transform (BFT). The main idea of this antijamming method is based on a three-step process: "parameter estimation—echo modulation—identification and suppression." The first step involves obtaining the delay and chirp rate of the jamming from the LVD matrix of the radar echo. Based on the estimated parameter information, a reference signal is designed to modulate the jamming into a complete chirp signal. In the second step, biorthogonal Fourier transform is used to distinguish between the target's echo and jamming based on the difference in the chirp rate. Finally, jamming is filtered using narrow-band filtering in the chirp rate domain, and the original echo is recovered by using biorthogonal inverse Fourier transform (IBFT). Simulation results demonstrate that the proposed method achieves high accuracy in estimating jamming parameters and is capable of suppressing false targets under high jamming-to-signal ratio (JSR) conditions.

1. Introduction

Smeared spectrum (SMSP) jamming [1] is a typical jamming pattern countering linear frequency modulation (LFM) radar [2], employing the digital radio frequency memory (DRFM) technique [3, 4]. The jamming technique involves intercepting the radar signal, modulating and splicing it with a specified delay. The resulting signal generates multiple false targets in a range after pulse compression processing, thus impeding the radar's ability to detect true targets and rendering the radar system ineffective.

Currently, two main methods are employed to suppress SMSP jamming: jamming cancellation and signal filtering [5]. The jamming cancellation method typically involves estimating the parameters of the jamming signal, reconstructing the signal, and then subtracting it from the echo to achieve jamming suppression [6–10]. However, estimating the jamming parameters accurately can be difficult, particularly under conditions of low signal-to-noise ratio (SNR), leading to poor suppression effectiveness. In contrast, the signal filtering method is achieved by transforming the jamming signal into other domains in which feature differences can be distinguished, and a suitable filter is designed to suppress it. For example, the authors of [11] use a two-dimensional fractional Fourier transform (FRFT) to identify and filter SMSP jamming signals by adjusting the transformation order, but the algorithm can be complex and computationally intensive. The author of [12] proposes a technique based on FRFT that can identify the differences between SMSP jamming and target echo based on their distinct chirp rate. After parameter estimation, by transmitting twin waveforms designed and modulating echo to carry out time-frequency shift, the authors of [13] convert the echo into conventional LFM signal and suppress

jamming through match filtering. However, the effect of jamming phase delay is not considered in [12, 13]. Another approach is to use the generalized S-transform to analyze the time-frequency distribution of the echo [14]. This method can identify the difference between the target echo and SMSP jamming, but its performance may be limited in low signal-to-noise ratio (SNR) environments.

In order to address the limitations of the antijamming techniques, we propose a novel approach that combines Lv's distribution (LVD) with biorthogonal Fourier transform (BFT) to effectively counter SMSP jamming effectively. Both LVD and BFT are powerful signal processing tools that are used in this paper for parameter estimation and jamming identification, respectively. LVD is a classical analytical tool widely used in the centroid frequency-chirp rate (CFCR) domain. The detection efficiency of the LFM signal by LVD is similar to that of the matching filter, and the parameter estimation accuracy is better than that of Wigner–Hough transform (WHT) and Radon-ambiguity transform (RAT) [15, 16]. LVD has been also applied to maneuvering target detection, radar image processing, communication system jamming suppression, and other fields. On the other hand, BFT is an effective time-frequency analysis tool employed in estimation of the chirp rate. The BFT algorithm is particularly suitable for the chirp rate analysis of multiple LFM signals with different chirp rates.

Our approach follows the concept of "parameter estimation—echo modulation—jamming identification and suppression." First, we extract the chirp rate and instantaneous frequency information from the LVD of the interfered echo signal and calculate the chirp rate and delay of SMSP jamming based on the LVD property. Next, we design a reference signal to modulate the jamming signal into a complete LFM signal. Then, BFT is used to identify the jamming signal and real target echo in the chirp rate domain, and narrow-band filtering is applied to suppress jamming. Finally, the real target echo is recovered by IBFT to complete the jamming suppression process. Our proposed technique has the potential to improve the effectiveness of SMSP jamming countermeasures and offers several advantages over existing methods. There are the following innovation points in this paper:

(1) LVD is applied to estimate the chirp rate and delay of interference signals innovatively in this paper. The accuracy and timeliness of parameter estimation are improved.

(2) The reference signal is designed to modulate the jamming signal into a complete LFM signal and to greatly reduce the difficulty of interference suppression.

(3) BFT is applied to identify the jamming signal and the real target echo by transforming disturbed echo into the chirp rate domain.

The structure of this paper is as follows: Section 2 presents an analysis of the characteristics of SMSP jamming. In Section 3, we provide a detailed description of the three steps that are used to suppress the jamming signal, namely, "parameter estimation, echo modulation, and jamming identification and suppression." In Section 4, we present the simulation results and compare the performance of our proposed method with other existing techniques. Finally, in Section 5, we draw our conclusions based on the findings of this study.

2. Analysis of SMSP Jamming Characteristics

2.1. Signal Models of SMSP Jamming. Radar transmits the LFM pulse, and the complex representation is

$$s(t) = \mathrm{rect}\left(\frac{t - T/2}{T}\right) e^{j\pi k t^2}, \tag{1}$$

where t represents the fast time, T represents the pulse duration of the transmitted signal, $k = B/T$ denotes the chirp rate, B represents the bandwidth, and $\mathrm{rect}(\cdot)$ is defined as

$$\mathrm{rect}(t) = \begin{cases} 0, & |t| > 0.5, \\ 0.5, & |t| = 0.5, \\ 1, & |t| < 0.5. \end{cases} \tag{2}$$

SMSP jamming consists of N LFM subwaveforms whose time width is T/N. The time-domain form of the first subwaveform is

$$j_1(t) = \mathrm{rect}\left(\frac{t - T/N/2}{T/N}\right) \mathrm{e}^{\mathrm{j}\pi k_j t^2}, \tag{3}$$

where $k_j = Nk$ represents the chirp rate of the subwaveform. We copy $j_1(t)N-1$ times consecutively to get SMSP jamming:

$$j(t) = \sum_{n=0}^{N-1} j_1\left(\frac{t - nT}{N}\right). \tag{4}$$

According to the time-shift property of Fourier transform, the expression of SMSP jamming in the frequency domain is obtained:

$$J(f) \approx \mathrm{rect}\left(\frac{f}{B} - \frac{1}{2}\right) \frac{\sin(\pi f T)}{\sin(\pi f T/N)} \mathrm{e}^{\mathrm{j}\pi/4 - \mathrm{j}\pi f^2/Nk - \mathrm{j}\pi f T} \mathrm{e}^{-\mathrm{j}\pi f T(1-1/N)}. \tag{5}$$

The output of SMSP jamming for pulse compression processing is

$$\begin{aligned} \mathrm{PC}_j(t) &= \int_0^B J(f) S^*(f) \mathrm{e}^{\mathrm{j}2\pi f t} \mathrm{d}f, \\ S^*(f) &\approx \frac{1}{\sqrt{k}} \mathrm{rect}\left(-\frac{f}{B} + \frac{1}{2}\right) \mathrm{e}^{\mathrm{j}\pi/4 + \mathrm{j}\pi f^2/k - \mathrm{j}\pi f T}, \end{aligned} \tag{6}$$

where $S^*(f)$ represents the spectrum of the matched filter.

2.2. Jamming Characteristic of SMSP Jamming. Under the self-protection jamming condition [17], the initial distance and speed of the jammer are set as R and v_t, respectively, and the angle between the velocity vector of the target and the radar main lobe is 0.

Then, the baseband signal of the real target (jammer) echo received by the radar is

$$s_r\left(t_f, t_m\right) = \sigma s\left[t_f - \frac{2R\left(t_m\right)}{c}\right] \mathrm{e}^{-\mathrm{j}4\pi R\left(t_m\right)/\lambda}, \tag{7}$$

where σ represents the reflection coefficient of the target, t_f and $t_m = mT_r$ represent the fast time and the slow time, respectively, and the fast time and the slow time represent the time of a pulse repetition period and the time of the continuous pulse repetition period, respectively. T_r represents the pulse repetition interval (PRI), $R(t_m) = R - v_t t_m$ represents the radial distance function between the jammer and radar, and c and λ represent the speed of light and wavelength.

The interfered echo signal received by the radar within a coherent processing interval (CPI) is

$$x_r\left(t_f, t_m\right) = \sigma s\left(t_f - \frac{2R_t}{c}\right) \mathrm{e}^{-\mathrm{j}4\pi R_t/\lambda} \mathrm{e}^{\mathrm{j}2\pi f_d t_m} + A_j j\left(t_f - \tau_r - \frac{2R_t}{c}\right) \mathrm{e}^{-\mathrm{j}4\pi R_t/\lambda} \mathrm{e}^{\mathrm{j}2\pi f_d t_m} + w\left(t_f, t_m\right), \tag{8}$$

where $f_d = 2v_t/\lambda$ represents the Doppler frequency, A_j represents the amplitude of SMSP jamming, R_t is consistent with $\mathbf{R}(t_m)$, τ_r represents the delay set by the jammer, and $w(t_f, t_m)$ represents the noise. Pulse compression of $x_r(t_f, t_m)$ can be obtained as

$$\mathrm{PC}\left(t_f, t_m\right) = \sigma T \,\mathrm{sinc}\left[\pi B\left(t_f - \frac{2R_t}{c}\right)\right] e^{-j4\pi R_t/\lambda} e^{j2\pi f_d t_m} + A_j \mathrm{PC}_j\left(t_f - \tau_r - \frac{2R_t}{c}\right) e^{-j4\pi R_t/\lambda} e^{j2\pi f_d t_m} + y_w\left(t_f, t_m\right), \tag{9}$$

where $PC_j(t_f)$ is consistent with $PC_j(t)$ in equation (6). According to equation (9), the real target echo after pulse compression generates the sinc pulses in the range axis, while SMSP jamming generates high-density false target peaks due to the change of the chirp rate. The jamming power is usually much larger than the target echo power, so the peak of the real target will be annihilated in jamming. Usually, a delay is set before forwarding, which plays a suppression effect within a certain range. The certain range is also known as the suppression distance, and the suppression distance usually overwrites the target distance. Therefore, it is also called the suppression distance, which is close to but not equal to the target distance.

In the following simulation, the radar has these parameters: The bandwidth and pulse duration of transmit signal are 8 MHz and 80 μs, respectively. The number of subwaveforms of SMSP jamming is 4. Target distance and suppression distance are 30 km and 32 km, respectively. Figure 1 shows the time-domain waveform and time-frequency distribution of SMSP jamming. Figure 2 shows the pulse compression results of echo with and without jamming. As can be seen from Figure 2, the real target after pulse compression has been completely submerged in jamming, making it difficult to achieve target detection.

3. The Suppression Methods of SMSP Jamming

The chirp rate is the greatest characteristic difference between SMSP jamming and target echo signal. However, SMSP jamming is composed of multiple LFM subwaveforms, and the chirp rate and delay are unknown in advance. So, it is impossible that the difference is used for jamming identification and suppression directly by using time-frequency tools such as FRFT and BFT. In this paper, LVD is used to estimate the chirp rate and delay of jamming. According to the above parameters, the reference signal is designed to modulate the jamming signal into a complete LFM signal. Then, jamming is identified by BFT and suppressed by narrow-band filtering in the chirp rate domain.

3.1. Parameter Estimation Method Based on LVD. At present, most jamming parameter estimation methods use time-frequency tools to analyze jamming signals, such as Wigner–Ville distribution (WVD) [18], short time Fourier transform (STFT) [19], and Radon–Wigner transform (RWT). But influenced by cross terms and time-frequency resolution, respectively, the effect is not ideal. LVD only requires a two-dimensional (2D) Fourier transform of a parametric scaled symmetric instantaneous autocorrelation function. It can be implemented by using the complex multiplications and fast Fourier transforms (FFTs) based on the scaling principle to get the chirp rate and the centroid frequency of the jamming signal. Therefore, LVD can reduce the computation amount in the parameter estimation process under the condition of equal accuracy.

Assume that the continuous multicomponent LFM signal $x(t)$ is represented as

$$x(t) = \sum_{i=0}^{\mathrm{K}-1} x_i(t) = \sum_{i=0}^{\mathrm{K}-1} A_i e^{j2\pi f_i t + j\pi k_i t^2}, \tag{10}$$

where K represents the number of signal components present in the signal, A_i represents the constant amplitude, f_i and k_i denote the centroid frequency and the chirp rate, respectively, and t is consistent with t_f in Section 2.1. According to the calculation method proposed in [16], the scale transformation of the parametric symmetric

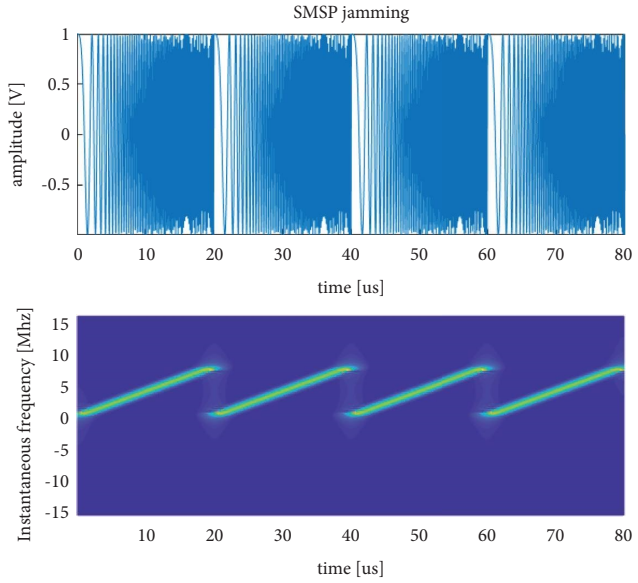

Figure 1: Time-domain waveform and time-frequency distribution of SMSP jamming.

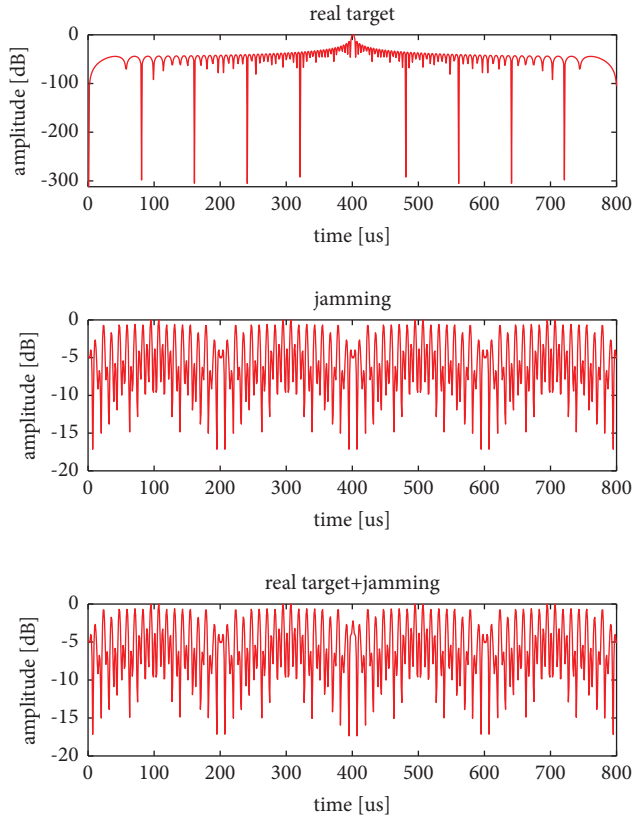

Figure 2: Pulse compression of the radar echo signal interfered by SMSP.

instantaneous autocorrelation function (PSIAF) of the signal $x(t)$ is carried out, so as to remove the similar coupling between the time variables. PSIAF is defined by

$$R_x^C(t,\tau) = x\left(t+\frac{\tau+a}{2}\right)x^*\left(t-\frac{\tau+a}{2}\right) = \sum_{i=0}^{\mathrm{K}-1} R_{x_i}^C(t,\tau) + \sum_{i=0}^{\mathrm{K}-2}\sum_{l=\mathrm{i}+1}^{\mathrm{K}-1}\left[R_{x_i x_l}^C(t,\tau) + R_{x_l x_i}^C(t,\tau)\right], \tag{11}$$

where τ denotes a lag variable and a denotes a constant time delay related to a scaling operator, the optimal value is usually 1 [16], $*$ denotes complex conjugation, and $R_{x_i}^C$ and $R_{x_i x_l}^C$ represent the auto terms and cross terms, respectively. PSIAF of equation (10) is given by

$$R_s^C(t,\tau) = \sum_{i=0}^{\mathrm{K}-1} A_i^2 \mathrm{e}^{\mathrm{j}2\pi f_i(\tau+a)+\mathrm{j}2\pi k_i(\tau+a)t} + \sum_{i=0}^{\mathrm{K}-2}\sum_{l=\mathrm{i}+1}^{\mathrm{K}-1}\left[R_{s_i s_l}^C(t,\tau) + R_{s_l s_i}^C(t,\tau)\right]. \tag{12}$$

In order to remove the similar coupling between t and τ, the scaling operator is defined by

$$t_n = (\tau+a)ht, \tag{13}$$

where t_n is called the scaled time and h is a scaling factor (the best performance is when the parameter is 1) [16]. Applying the scaling operator to (12), we have

$$R_s^C(t_n,\tau) = \sum_{i=0}^{\mathrm{K}-1} A_i^2 \mathrm{e}^{\mathrm{j}2\pi f_i(\tau+a)+\mathrm{j}2\pi\left(k_i/h\right)t_n} + \sum_{i=0}^{\mathrm{K}-2}\sum_{l=\mathrm{i}+1}^{\mathrm{K}-1}\left[R_{s_i s_l}^C(t_n,\tau) + R_{s_l s_i}^C(t_n,\tau)\right]. \tag{14}$$

By performing 2D Fourier transformation on equation (14), we obtain the LVD defined by

$$L_x(f,r) = \underbrace{\sum_{i=0}^{\mathrm{K}-1} L_{x_i}(f,r)}_{\text{auto terms}} + \underbrace{\sum_{i=0}^{\mathrm{K}-2}\sum_{l=\mathrm{i}+1}^{\mathrm{K}-1} L_{x_i x_l}(f,r)}_{\text{cross terms}}, \tag{15}$$

$$L_{x_i}(f,r) = A_i^2 \mathrm{e}^{\mathrm{j}2\pi a f}\delta(f-f_i)\delta\left(r-\frac{k_i}{h}\right), \tag{16}$$

where f and k represent the centroid frequency and chirp rate of the signal. Although equation (14) shows that there also exist the cross terms on the LVD plane, they are much smaller than the auto terms [16]. So, the effect of cross terms can be ignored here. According to the frequency and chirp rate shift of LVD [16],

$$x(t-t_0) \Longleftrightarrow \mathrm{LVD}\left(f+kt_0-f_i, r-\frac{k_i}{h}\right)\mathrm{e}^{\mathrm{j}2\pi\left(f_i a-\mathrm{k}a t_0\right)}. \tag{17}$$

The chirp rate and delay of jamming signals can be estimated according to equations (16) and (17):

$$r-\frac{k_i}{h} = 0 \Longrightarrow k_j = k^{'}\ (h=1), \tag{18}$$

$$f+kt_0-f_i = 0 \Longrightarrow t_0 = \frac{\left|f_1-f_s\right|}{k^{'}}, \tag{19}$$

where $k^{'}$ represents the chirp rate axis coordinate of the jamming peak in LVD distribution and f_1 and f_s represent the centroid frequency axis coordinate of the first jamming's peak and target echo peak. In formulas (18) and (19), r and h represent the peak coordinates of the SMSP subsignal and target echo signal in LVD.

Taking SFT-IFFT as the realization method of LVD discretization calculation [16], the computational complexity is compared. Let P be the number of time samples and Q be the number of lag samples. Assuming that the calculation of FFT over n requires the computational costs in the order of $O(P\log P)$, the computational costs of SFT-IFFT are $O(4PQ\log P)$. Since LVD is 2D-FFT of PSIAF, the overall complexities of the LVD are $O(4QP\log P + QP\log P + QP\log Q)$, which is in order of $O(P^2\log P)$

under the assumption of $P = Q$. For RWT, the dechirping computational cost is in the order of $O(Q'P\log P)$, where Q' is the number of projection angles, offering significant computation advantage over $O(Q'P^2)$ for the direct projection [20]. It can be seen that the computational load of LVD based on SFT-IFFT is equivalent to those of RWT by dechirping. However, according to [16], the calculation accuracy of RWT is low in time-frequency analysis, while the resolution of LVD is much higher than that of RWT. It should be noted that LVD can estimate the chirp rate and the jamming delay at the same time without repeating the calculation.

Taking $N = 4$ as an example, Figure 3 shows the distribution diagram of the LVD of disturbed echo.

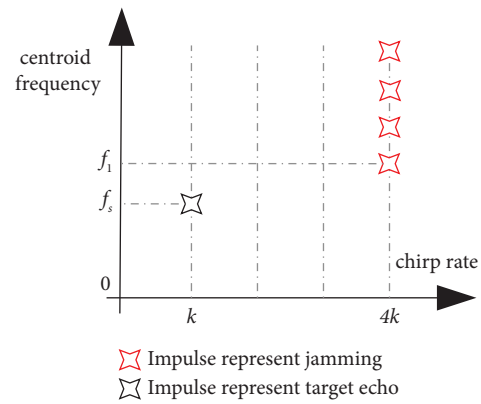

Figure 3: The LVD of disturbed echo.

3.2. Methods of Echo Modulation. The instantaneous frequency of the disturbed echo signal can be expressed as

$$f(t) = \mathrm{rect}\left(\frac{t - T/2}{T}\right)kt + \sum_{n=0}^{N-1}\mathrm{rect}\left[\frac{(t-\tau_r) - T/N/2 - nT/N}{T/N}\right]\left[Nk(t-\tau_r) - nB\right]. \tag{20}$$

In order to modulate the jamming signal into a complete LFM signal, the instantaneous frequency of the reference signal is expressed as

$$f_{\mathrm{ref}}(t) = \sum_{n=0}^{N-1}\mathrm{rect}\left[\frac{(t-\tau_r) - T/N/2 - nT/N}{T/N}\right]nB. \tag{21}$$

The reference signal designed is expressed as

$$s_{\mathrm{ref}}(t) = \sum_{n=0}^{N-1}\mathrm{rect}\left[\frac{(t-\tau_r) - T/N/2 - nT/N}{T/N}\right]e^{\left[\mathrm{i}2\pi nB(t-\tau_r)\right]}. \tag{22}$$

The reference signal $s_r(t)$ is used to modulate the jamming signal, so the real target echo and jamming after modulation are

$$\begin{aligned} s'(t) &= \sigma\sum_{n=0}^{N-1}\mathrm{rect}\left[\frac{(t-\tau_r) - T/N/2 - nT/N}{T/N}\right]e^{\mathrm{j}2\pi nB(t-\tau_r)}e^{\mathrm{j}\pi kt^2}, \\ j'(t) &= A_j\mathrm{rect}\left[\frac{(t-\tau_r) - T/2}{T}\right]e^{\mathrm{j}\pi Nk(t-\tau_r)^2}. \end{aligned} \tag{23}$$

The modulated SMSP jamming is an LFM signal with a time width of T and bandwidth of NB (the Doppler frequency of jamming is ignored here for the convenience of analysis). Figure 4 shows the schematic diagram of modulation of SMSP jamming when $N = 4$.

3.3. Method of Jamming Identification and Suppression. BFT uses biorthogonal function expansion for signals to obtain the chirp rate density spectrum of signals [21]. A single LFM signal will generate a sinc function pulse in the chirp rate axis after BFT processing. Therefore, BFT has a special advantage in processing multicomponent LFM signals with a chirp rate difference.

The definition of BFT is

$$\mathrm{BFT}[s(t)]\colon F(\omega_2) = 2\int_0^{+\infty} s(t)te^{-\mathrm{j}\pi\omega_2 t^2}\mathrm{d}t. \tag{24}$$

Therefore, the BFT result of the radar transmitted signal is given by

$$\mathrm{BFT}[s(t)] = T^2\left|\mathrm{sinc}\left[\frac{\pi T^2}{2}(\omega_2 - k)\right]\right|. \tag{25}$$

According to equation (25) and Taylor's expansion equation, the BFT result of radar transmitted signal with carrier frequency f_0 is obtained:

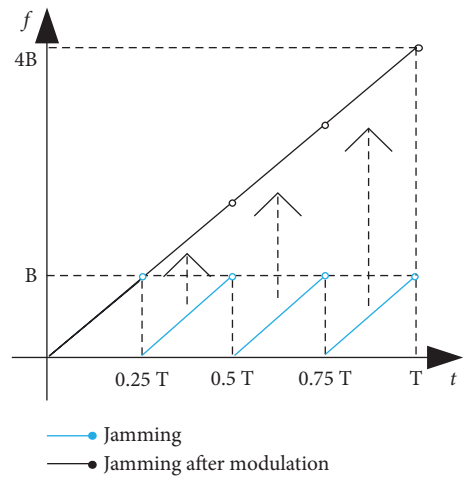

Figure 4: Modulation of SMSP jamming.

$$\begin{aligned}\mathrm{BFT}\left[s(t)e^{j2\pi f_0 t}\right] &= 2\int_0^{T_p} e^{j2\pi f_0 t} e^{j\pi(k-\omega_2)t^2} dt^2, \\ &\approx T^2\left|\mathrm{sinc}\left[\frac{\pi T^2}{2}\left(\omega_2 - k - \frac{f_0}{B}k\right)\right]\right|.\end{aligned} \tag{26}$$

According to the time-shift property and frequency-shift property of BFT combined with equation (26), the BFT results of the real target echo and jamming signal are obtained:

$$|\mathrm{BFT}[s(t)]| \approx \sigma T^2\left|\mathrm{sinc}\left[\frac{\pi T^2}{2}\left(\omega_2 - k - \frac{f_0}{B}k + \frac{t_0}{T}k\right)\right]\right|, \tag{27}$$

$$|\mathrm{BFT}[j(t)]| \approx \mathrm{AT}^2\left|\mathrm{sinc}\left[\frac{\pi T^2}{2}\left(\omega_2 - Nk - \frac{f_0}{B}k + \frac{t_0+\tau}{T}Nk\right)\right]\right|, \tag{28}$$

where A represents the altitude of jamming. It can be seen from equations (26) and (27) that after BFT processing, the sinc function pulse of the real target echo and jamming signal are located at $\omega_2 = k + f_0/Bk - t_0/Tk \approx k$ and $\omega_2 = Nk + f_0/Bk - t_0 + \tau/TNk \approx Nk$, respectively. Figure 5 shows the schematic diagram of the BFT results of the disturbed echo.

In order to filter out jamming signals, a filtering window is designed to perform narrow-band filtering on the location of jamming peaks:

$$\widetilde{F}(\omega_2) = \left|\mathrm{BFT}\left[s'(t) + j'(t)\right]\right|\mathrm{win}(\omega_2), \tag{29}$$

where (ω_2) represents function of the filtering window. The actual operation is to assign the value of 0 to the data in the specified coordinate range. Then, the target echo signal can be recovered by IBFT:

$$s''(t) = \mathrm{IBFT}\left[\widetilde{F}(\omega_2)\right]. \tag{30}$$

The echo is demodulated after filtering jamming. Finally, the target information is extracted by pulse compression and phase-coherent accumulation. Based on Sections 3.1~3.3, Figure 6 shows the suppression process of SMSP jamming.

4. Simulation

In the following simulation, the radar and SMSP jamming have the same parameter values mentioned in Section 2.

Figure 7 shows the BFT result of the SMSP jamming and target echo signal without setting the suppression distance and with setting the suppression distance. A jamming-to-signal ratio (JSR) here is set at 5 dB for better effects.

We can see there are sinc peaks at 100 GHz/s and 400 GHz/s, respectively, on the chirp rate axis generated by the target echo and jamming signal, but the results are not always ideal. Figure 7 verifies the necessity of parameter estimation and echo modulation mentioned in Sections 3.1 and 3.2. At first, jamming with setting the suppression distance cannot generate the sinc peak in the chirp rate domain through BFT, because the performance of the BFT is best when the initial frequency of the LFM signal is zero. Second, SMSP jamming is an incomplete LFM signal, and the initial frequency of the last three jamming segments is not 0, so there will be too large number of clutter in the chirp rate axis to identify the peak generated by target echo.

In summary, there are two reasons for the large number of peak outputs. On the one hand, because the echo is not intercepted according to the jamming delay, the initial

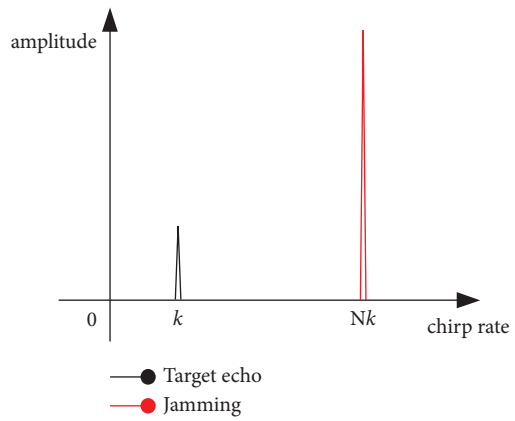

Figure 5: The BFT result of the disturbed echo.

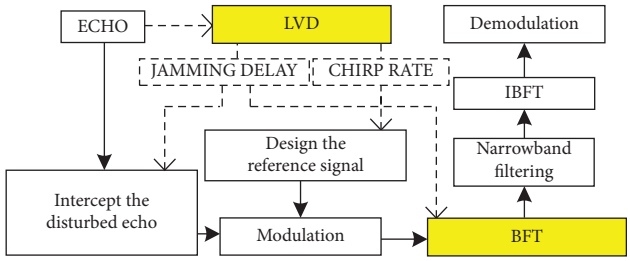

Figure 6: Suppression process of SMSP jamming.

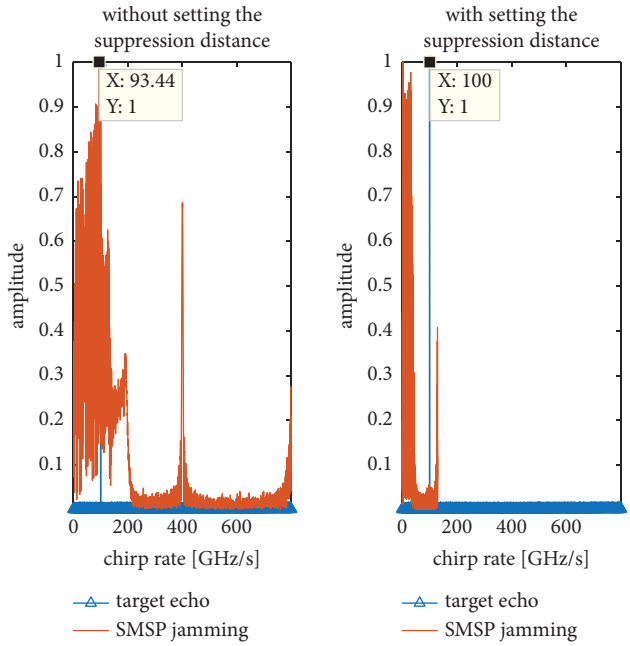

Figure 7: BFT result of radar echo signal interfered by SMSP.

frequency of the signal is not 0. On the other hand, the SMSP jamming is not modulated, and the last three jammer signals cannot generate the sinc peak.

4.1. Simulation Analysis of Jamming Suppression Algorithm. The jamming suppression method is analyzed and verified in this section. The parameters of the LFM pulse signal and jamming are consistent with those in Section 2.

First, we use LVD to estimate the jamming parameters. Figure 8 shows the LVD of disturbed echo. Then, the reference signal is designed to modulate the jamming signal according to the estimation of the chirp rate and delay. Figure 9 shows the time-frequency distribution diagram of the modulated echo.

It can be seen from Figure 8 that the estimated chirp rate is basically consistent with the real parameters. According to the frequency axis coordinates shown in the figure, the suppression distance of jamming can be obtained as 1.989 km by inserting them into (18). As can be seen from Figure 9, after modulation, the jamming signal is a complete LFM signal, while the target echo signal appears as frequency transition.

Next, BFT is used to process the modulated echo signal. The BFT result of the modulated echo signal is shown in Figure 10. It can be seen from Figure 10 that the jamming signal after modulation generates a peak whose value is much larger than the peak generated by target echo, and the chirp rate of jamming and real target are consistent with the simulation parameters.

At last, the peak generated by jamming is filtered by narrow-band filtering, and the real target echo is recovered by IBFT. Figure 11 shows the time-frequency distribution of the recovered signal. By comparing Figures 9 and 11, it can be seen that only a little part of the jamming signal remains, and the amplitude of the residual part is greatly reduced. Meanwhile, the real target echo is retained well.

4.2. Simulation Analysis of Algorithm Efficiency

4.2.1. Simulation of Jamming Parameter Estimation. In order to analyze the accuracy of chirp rate estimation, the parameters estimation accuracy (PEA) of chirp rate estimation is defined:

$$\mathrm{PEA}_{\mathrm{chirprate}} = \frac{1}{\mathrm{MTK}} \sum_{i=1}^{\mathrm{MTK}} \left(1 - \frac{\left|k - k_i'\right|}{k}\right), \tag{31}$$

where MTK is the number of Monte Carlo simulations and k_i' is the estimated chirp rate of the ith Monte Carlo simulation. The values of SNR are −10 dB, −5 dB, and 0 dB,

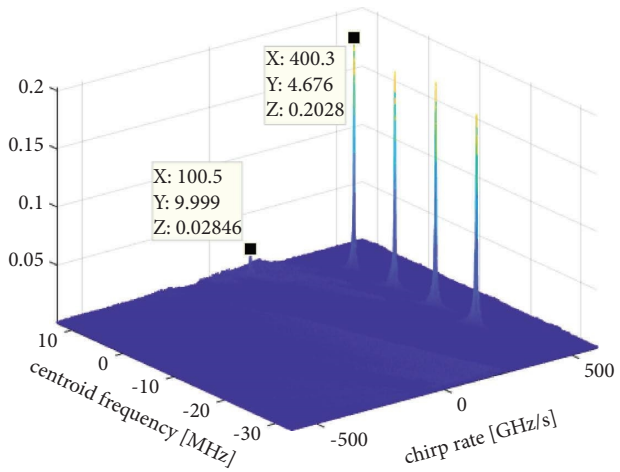

Figure 8: The LVD of interfered echo.

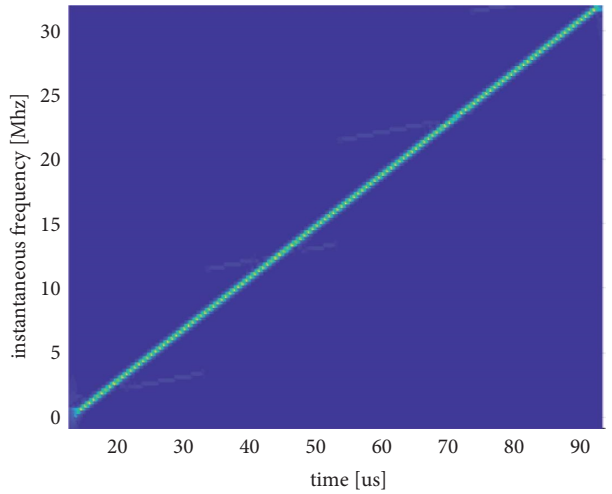

Figure 9: Time-frequency distribution diagram of the modulated echo.

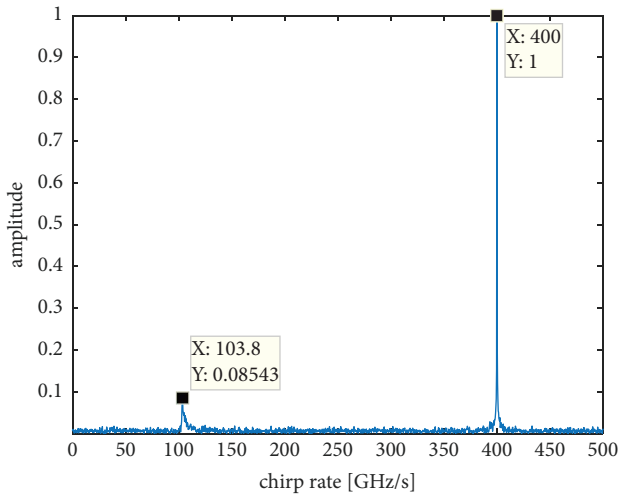

Figure 10: The result of the BFT.

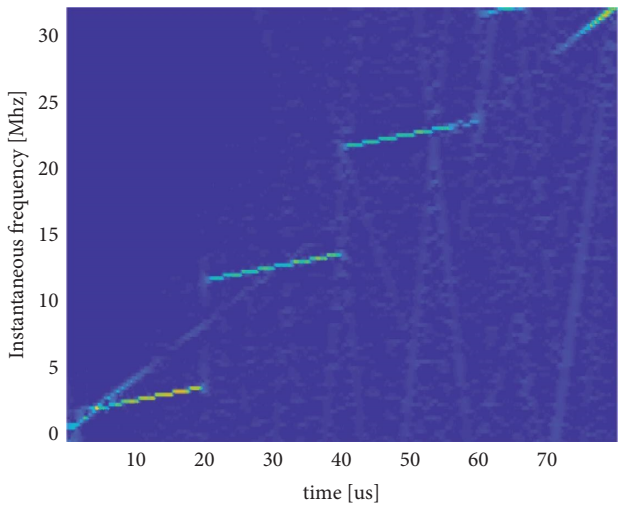

Figure 11: The time-frequency distribution of the recovered signal.

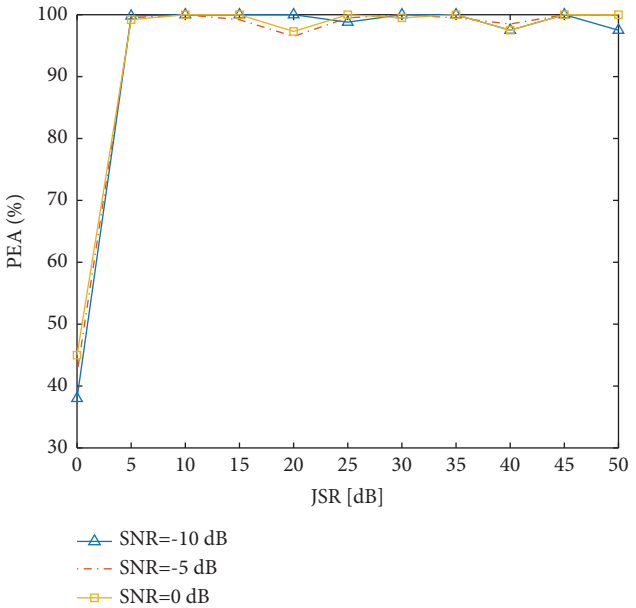

Figure 12: PEA of chirp rate estimation.

respectively, and the JSR increases from 0 dB to 50 dB at intervals of 5 dB. The results of 100 Monte Carlo simulations are shown in Figure 12. It can be seen that the accuracy of chirp rate estimation is almost unaffected by SNR. PEA can reach 100% when JSR is higher than 5 dB.

In order to analyze the estimation accuracy of jamming delay, PEA of delay estimation is defined:

$$\mathrm{PEA}_{\mathrm{delay}} = \frac{1}{\mathrm{MTK}} \sum_{i=1}^{\mathrm{MTK}} \left(1 - \frac{\left|t_0 - t_i'\right|}{t_0}\right), \tag{32}$$

where t_0 and t_i' are the time-domain sampling point corresponding to the real jamming front and the estimated front. The values of SNR are −10 dB, −5 dB, and 0 dB, respectively, and the JSR increases from 0 dB to 50 dB at intervals of 5 dB. The result of 100 Monte Carlo simulations is

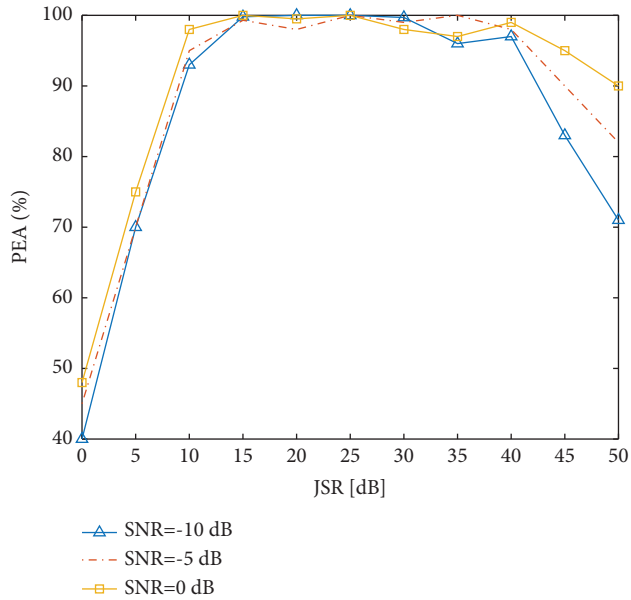

Figure 13: PEA of delay estimation of jamming.

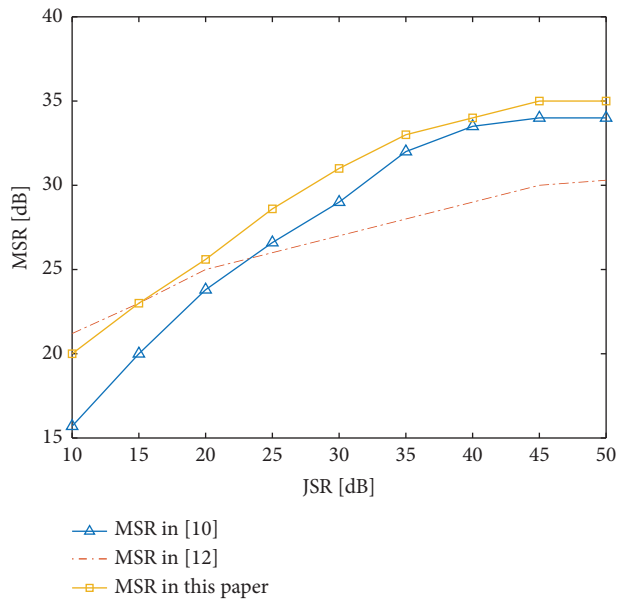

Figure 14: The curve of MSR with JSR.

shown in Figure 13. As can be seen from Figure 13, the estimation accuracy is no less than 90% when JSR is within the range of 10–40 dB. Too small or too large JSR will affect the accuracy of estimation. When JSR is too small, the accuracy will be affected by the estimation accuracy of the chirp rate. When JSR is too large and SNR is low, the peak generated by the real target echo in LVD may be submerged in the noise, resulting in the decline of the accuracy.

4.2.2. Performance Analysis of the Jamming Suppression Method. In this section, the mean suppression ratio (MSR) is used as the evaluation index to analyze the jamming suppression efficiency. We define the jamming MSR as

$$\mathrm{MSR} = \frac{1}{\mathrm{MTK}} \sum_{i=1}^{\mathrm{MTK}} \left(\mathrm{JSR}_{ij} - \mathrm{JSR}'_{ij}\right), \tag{33}$$

where JSR_i and JSR'_i are the JSR without jamming suppression and after jamming suppression in the ith Monte Carlo simulation, respectively. The SNR value is −5 dB, JSR increased from 10 dB to 50 dB at intervals of 5 dB, and the Monte Carlo simulation is run 100 times. Figure 14 shows the curve of MSR with JSR compared with [10, 12]. As shown in Figure 14, when JSR is greater than 20 dB, the MSR curve of [12] is flatter than that of the other two methods. The method proposed in this paper is slightly inferior to [12] only when JSR is lower than 15 dB. In summary, the proposed method has good comprehensive performance.

5. Conclusion

Aiming at SMSP jamming, this paper proposes a method combining LVD with BFT to suppress jamming, which realizes the idea "parameter estimation, echo modulation, jamming identification, and narrow-band filtering." Simulation results show that LVD can accurately estimate the chirp rate and jamming delay. The estimation accuracy of the chirp rate can approach 100% when JSR is larger than 5 dB, and the estimation accuracy of jamming delay can approach 100% when JSR is larger than 10−40 dB. The effectiveness of the suppression algorithm is verified by analyzing the mean suppression ratio. The comprehensive performance of the proposed algorithm is slightly better than that of the compared methods.

Data Availability

The raw/processed data required to reproduce these findings cannot be shared at this time as the data also form part of an ongoing study.

Disclosure

The statements, opinions, and data contained in all publications are solely those of the individual author(s) and contributor(s) and not of MDPI and/or the editor(s). MDPI and/or the editor(s) disclaim responsibility for any injury to people or property resulting from any ideas, methods, instructions, or products referred to in the content.

Conflicts of Interest

The authors declare that they have no conflicts of interest.

Acknowledgments

This research was funded by the National Natural Science Foundation of China under Grant no. 61731023 and the Shandong Provincial Natural Science Foundation of China under Grant no. ZR2020MF015.

References

[1] J. Sparrow and J. Cakilo, "ECM techniques to counter pulse compression radar," ITT Manufacturing Enterprises Inc, New York, NY, USA, United States Patent 7081846, 2006.

[2] M. I. Skolink, *Introduction to Radar Systems*, McGraw-Hill Book Co, New York, NY, USA, 2004.

[3] S. D. Berger, "Digital radio frequency memory linear range gate stealer spectrum," *IEEE Transactions on Aerospace and Electronic Systems*, vol. 39, no. 2, pp. 725–735, 2003.

[4] M. Greco, F. Gini, and A. Farina, "Radar detection and classification of jamming signals belonging to a cone class," *IEEE Transactions on Signal Processing*, vol. 56, no. 5, pp. 1984–1993, 2008.

[5] L. Ding, R. Li, Y. Wang, L. Dai, and F. Chen, "Discrimination and identification between mainlobe repeater jamming and target echo by basis pursuit," *IET Radar, Sonar & Navigation*, vol. 11, no. 1, pp. 11–20, 2017.

[6] X. Li, C. Wang, and H. Yuan, "SMSP jamming suppression method based on jamming reconstruction and kurtosis maximum," *Journal of Beijing University of Aeronautics and Astronautics*, vol. 44, no. 06, pp. 63–71, 2018.

[7] H. Yuan, C. Y. Wang, and L. An, "Smeared spectrum jamming suppression method based on signal reconstruction," *Journal of Systems Engineering and Electronics*, vol. 39, no. 5, pp. 961–967, 2017.

[8] L. Zhang, G. H. Wang, and X. Y. Zhang, "Fast-Slow time domain joint processing suppressing smeared spectrum Jamming," *Journal of Electronics & Information Technology*, vol. 42, no. 10, pp. 2508–2515, 2020.

[9] J. Ren and P. Wang, "Novel smart noise jamming suppression method based on smeared spectrum," *Progress In Electromagnetics Research Letters*, vol. 67, pp. 81–88, 2017.

[10] C. Wu, B. Chen, M. Yang, and M. Dong, "A study on parameter estimation and suppression for smeared spectrum jamming based on short-time Fourier transform," *EURASIP Journal on Wireless Communications and Networking*, vol. 2020, p. 115, 2020.

[11] L. Zhang, G. H. Wang, and X. Y. Zhang, "Smeared spectrum jamming suppression algorithm based on multiple orders 2D-FRFT," *Acta Armamentarii About the Journal*, vol. 41, no. 09, pp. 1826–1836, 2020.

[12] B. S. Samer, "Countering self-protection smeared spectrum jamming against chirp radars," *IET Radar, Sonar & Navigation Call for Papers*, vol. 15, no. 4, pp. 382–389, 2021.

[13] Z. D. Liu, Q. Zhang, and Y. Luo, "A smeared spectrum interference suppression method based on twinwaveform design," *Acta Aeronautica et Astronautica Sinica*, vol. 43, no. 02, pp. 352–361, 2022.

[14] X. Li, C. Wang, M. Tan, and X. Fu, "Smeared spectrum jamming suppression based on generalized S transform and threshold segmentation," *AIP Conference Proceedings*, vol. 1955, no. 1, pp. 140–147, 2018.

[15] X. L. Lv, M. D. Xing, S. H. Zhang, and Z. Bao, "Keystone transformation of the Wigner-Ville distribution for analysis of multicomponent LFM signals," *Signal Processing*, vol. 89, no. 5, pp. 791–806, 2009.

[16] X. L. Lv, G. A. Bi, C. R. Wan, and M. Xing, "Lv's distribution: principle, implementation, properties, and performance," *IEEE Transactions on Signal Processing*, vol. 59, no. 8, pp. 3576–3591, 2011.

[17] D. Adamy and L. Ew, *104: Electronic Warfare against a New Generation of Threats*, Artech House, Norwood, MA, USA, 2015.

[18] Y. Wu and X. Li, "Elimination of cross-terms in the Wigner–Ville distribution of multi-component LFM signals," *IET Signal Processing*, vol. 11, no. 6, pp. 657–662, 2017.

[19] I. Djurovie, V. Popovic-Bugarin, and M. Simeunovic, "The STFT-based estimator of Micro-Doppler parameters," *IEEE Transactions on Aerospace and Electronic Systems*, vol. 53, no. 3, pp. 1273–1283, 2017.

[20] J. C. Wood and D. T. Barry, "Radon transformation of time-frequency distributions for analysis of multicomponent signals," *IEEE Transactions on Signal Processing*, vol. 42, no. 11, pp. 3166–3177, 1994.

[21] B. Q. Wang and X. G. Li, "Analysis algorithm to frequency rate of LFM signal based on biorthogonal Fourier transform," *Journal of Electronics And Information*, vol. 31, no. 7, pp. 1620–1623, 2009.